Acta Biomaterialia 111 (2020) 267–278

Contents lists available at ScienceDirect

Acta Biomaterialia

journal homepage: www.elsevier.com/locate/actbio

Early changes in cartilage pericellular matrix micromechanobiology portend the onset of post-traumatic osteoarthritis ☆

Daphney R. Chery[1], Biao Han[1], Qing Li[1], Ying Zhou[2], Su-Jin Heo[3,4], Bryan Kwok[1], Prashant Chandrasekaran[1], Chao Wang[1], Ling Qin[3], X. Lucas Lu[5], Dehan Kong[2], Motomi Enomoto-Iwamoto[6], Robert L. Mauck[3,4], Lin Han[1,*]

[1] School of Biomedical Engineering, Science and Health Systems, Drexel University, Philadelphia, PA 19104, United States
[2] Department of Statistical Sciences, University of Toronto, Toronto, ON M5S 3G3, Canada
[3] McKay Orthopaedic Research Laboratory, Department of Orthopaedic Surgery, Perelman School of Medicine, University of Pennsylvania, Philadelphia, PA 19104, United States
[4] Translational Musculoskeletal Research Center, Corporal Michael J. Crescenz Veterans Administration Medical Center, Philadelphia, PA 19104, United States
[5] Department of Mechanical Engineering, University of Delaware, Newark, DE 19716, United States
[6] Department of Orthopaedics, School of Medicine, University of Maryland, Baltimore, MD 21201, United States

ARTICLE INFO

Article history:
Received 3 December 2019
Revised 2 May 2020
Accepted 5 May 2020
Available online 16 May 2020

Keywords:
pericellular matrix
chondrocyte mechanotransduction
post-traumatic osteoarthritis
nanomechanics
calcium signaling

ABSTRACT

The pericellular matrix (PCM) of cartilage is a structurally distinctive microdomain surrounding each chondrocyte, and is pivotal to cell homeostasis and cell-matrix interactions in healthy tissue. This study queried if the PCM is the initiation point for disease or a casualty of more widespread matrix degeneration. To address this question, we queried the mechanical properties of the PCM and chondrocyte mechanoresponsivity with the development of post-traumatic osteoarthritis (PTOA). To do so, we integrated Kawamoto's film-assisted cryo-sectioning with immunofluorescence-guided AFM nanomechanical mapping, and quantified the microscale modulus of murine cartilage PCM and further-removed extracellular matrix. Using the destabilization of the medial meniscus (DMM) murine model of PTOA, we show that decreases in PCM micromechanics are apparent as early as 3 days after injury, and that this precedes changes in the bulk ECM properties and overt indications of cartilage damage. We also show that, as a consequence of altered PCM properties, calcium mobilization by chondrocytes in response to mechanical challenge (hypo-osmotic stress) is significantly disrupted. These aberrant changes in chondrocyte micromechanobiology as a consequence of DMM could be partially blocked by early inhibition of PCM remodeling. Collectively, these results suggest that changes in PCM micromechanobiology are leading indicators of the initiation of PTOA, and that disease originates in the cartilage PCM. This insight will direct the development of early detection methods, as well as small molecule-based therapies that can stop early aberrant remodeling in this critical cartilage microdomain to slow or reverse disease progression.

Statement of Significance

Post-traumatic osteoarthritis (PTOA) is one prevalent musculoskeletal disease that afflicts young adults, and there are no effective strategies for early detection or intervention. This study identifies that the reduction of cartilage pericellular matrix (PCM) micromodulus is one of the earliest events in the initiation of PTOA, which, in turn, impairs the mechanosensitive activities of chondrocytes, contributing to the vicious loop of cartilage degeneration. Rescuing the integrity of PCM has the potential to restore normal chondrocyte mechanosensitive homeostasis and to prevent further degradation of cartilage. Our findings enable the development of early OA detection methods targeting changes in the PCM, and treatment strategies that can stop early aberrant remodeling in this critical microdomain to slow or reverse disease progression.

https://doi.org/10.1016/j.actbio.2020.05.005
1742-7061/

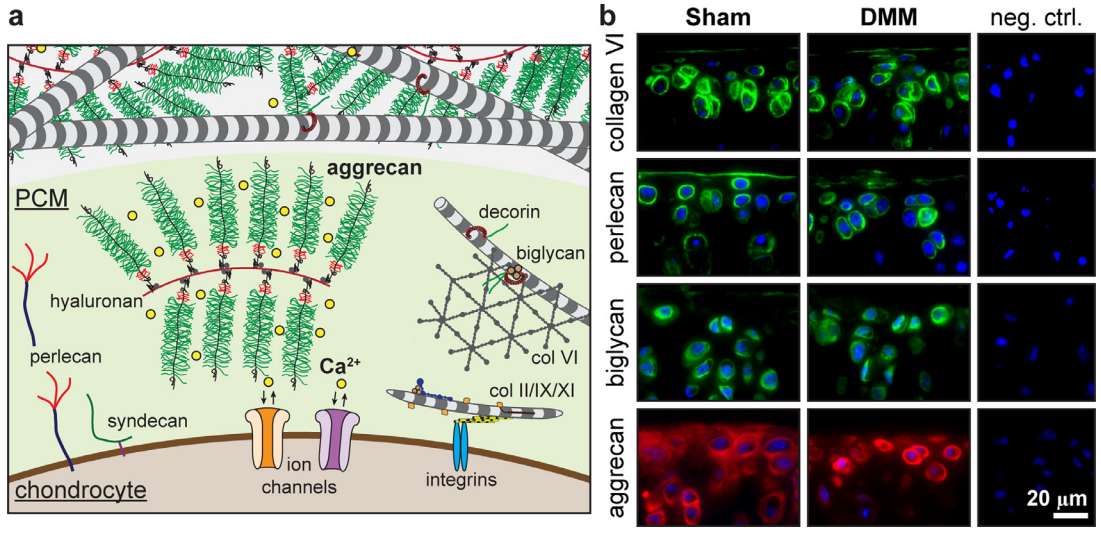

Fig. 1. a) Schematic illustration of cartilage matrix molecular constituents highlighting the distinctive structure and composition of the PCM in comparison to the T/IT-ECM, as well as the pivotal role of the PCM in mediating cell-matrix interactions. The schematic is inspired by Ref. [7, 10]. **b)** Representative immunofluorescence images of matrix molecules that are localized or preferentially distributed in the PCM at 8 weeks post-surgery, including collagen VI, perlecan, biglycan (green) and aggrecan (red; blue: DAPI). Internal negative controls are shown in the right panel.

1. Introduction

Post-traumatic osteoarthritis (PTOA) is characterized by the breakdown of cartilage following injury, such as meniscus and/or anterior cruciate ligament (ACL) tears. In contrast to spontaneous OA, PTOA is particularly prevalent in young adults, resulting in a long-term detrimental influence on quality of life [1]. Currently, there are no effective strategies for early detection or intervention of PTOA [2]. This is due, in part, to our limited understanding of the molecular and cellular events that contribute to the initiation of the disease. One hallmark of PTOA is the disrupted cross-talk between cells and the extracellular matrix (ECM) in which they reside, leading to imbalance in their anabolic and catabolic activities [3, 4]. An elevation in chondrocyte catabolism, without an offsetting increase in anabolic activities, results in the degradation of ECM constituents and ultimately compromises the overall tissue mechanical properties. This, in turn, further disrupts the mechanically regulated chondrocyte homeostasis, leading to a vicious loop of irreversible cartilage degeneration [5].

Chondrocytes reside within the pericellular matrix (PCM), a ~ 2-4 μm-thick intermediary layer between the cell and the further-removed, territorial/interterritorial domain of the ECM (T/IT-ECM) [6-8] (Fig. 1a). The composition, structure and biomechanical properties of the PCM are distinct from that of the T/IT-ECM [9, 10]. Given its immediate contact with cells , the PCM plays critical roles in sequestering growth factors [11], transducing mechanoelectrochemical signals [12, 13], and modulating ECM-cell strain transmission [14-16]. The importance of the PCM is underscored by the substantial cartilage phenotype seen in mice lacking PCM-specific molecules, such as collagen type VI [17, 18], perlecan [19] and biglycan [20]. Also, given that it makes direct contact with cells, the PCM is highly sensitive to chondrocyte metabolism. Aggrecan, the major cartilage matrix proteoglycan, undergoes much faster turnover in the PCM than in the T/IT-ECM [21], and newly synthesized aggrecan is primarily localized in the PCM [22]. In OA, aggrecan is the first matrix constituent to undergo degradation [23]. In human OA cartilage specimens, the PCM shows a marked reduction in properties [24, 25]. Thus, the PCM is potentially a key player in OA pathogenesis [7]. However, it is unclear whether the aberrant degradative processes that eventuate in disease are initiated at the level of cell-ECM interactions or the role that this PCM microdomain plays in PTOA.

This study sought to elucidate the role of PCM biomechanics and chondrocyte mechanotransduction in the initiation and progression of PTOA. Given the immediacy of PCM-cell contact, we hypothesize that degradation of the PCM is one of the earliest events seen upon the initiation of OA, and this, in turn, leads to disrupted chondrocyte mechanotransduction. To test this hypothesis, we investigated changes of PCM microscale modulus and chondrocyte intracellular calcium signaling over a well-defined time frame following injury. Specifically, we adapted the destabilization of the medial meniscus (DMM) murine surgical model [26], one of the most widely used models for studying PTOA development in vivo [27]. Using this model, we recently showed that the bulk cartilage tissue modulus is reduced as early as 1 week after DMM, well before histological evidences of disease, illustrating the centrality of mechanical changes in disease onset [28]. Building on this work, here, we studied the longitudinal changes of PCM micromodulus starting from 3 days after DMM up to 8 weeks, when histological signs of PTOA became apparent [26]. Furthermore, we queried the changes in chondrocyte baseline and mechanically instigated intracellular calcium signaling ($[Ca^{2+}]_i$), which is one of the earliest, fundamental cell responses to mechanical stimuli [29], and is commonly used as a marker of chondrocyte mechanosensitive activities [30]. Our findings demonstrate rapid changes in PCM integrity and chondrocyte mechanotransduction during PTOA initiation, which could be blocked by early inhibition of PCM remodeling. These data provide a novel target for developing early detection and therapeutics to identify and arrest disease initiation.

2. Methods

2.1. Animal surgery

Destabilization of the medial meniscus (DMM) surgery was performed on the right hind knees of 12-week old C57BL/6 wild-type (WT) male mice (Jackson Laboratory, Bar Harbor, ME), following established procedures [26]. Sham control surgery was performed on

☆ For submission to *Acta Biomaterialia* as a *Full-length Article.*

* Correspondence and requests for materials should be addressed to: Dr. Lin Han, Phone: (215) 571-3821, Fax: (215) 895-4983

E-mail address: lh535@drexel.edu (L. Han).

contralateral left knees. Mice were euthanized at 3 days, 1 week, 2 weeks and 8 weeks after surgery ($n = 8$ at each time point for AFM nanomechanical mapping and $[Ca^{2+}]_i$ signaling studies, except for $n = 10$ for the 3-day time point, and additional $n = 14$ at the 1-week time point for treatment studies, $n = 4$ at the 8-week time point for immunofluorescence imaging). All animal work was approved by the Institutional Animal Care and Use Committee (IACUC) at Drexel University.

2.2. Immunofluorescence imaging of matrix molecules

To determine if the PCM retains its morphological integrity and compositional distinction from the T/IT-ECM within the tested time frame post-DMM (Fig. 1a), we assessed the distribution of the major proteoglycan, aggrecan, and other molecules that are specific to the PCM at 8 weeks post-surgery ($n = 4$, Fig. 1b). Immediately after euthanasia, whole joints of both Sham and DMM knees were harvested, fixed in 4% paraformaldehyde, and decalcified in 10% EDTA for 21 days. Samples were embedded in paraffin and serial 6-μm thick sagittal sections were cut across the joint. Following established protocols [31], sections were incubated with the primary antibodies in 1% bovine serum albumin (BSA), 1 × PBS for collagen VI (70R-CR009X, Fitzgerald, Acton, MA, 1:200 dilution), perlecan (A7L6, Santa Cruz Biotech, Dallas, TX, 1:200), biglycan (ABT271, MilliporeSigma, Burlington, MA, 1:100) and aggrecan (AB1031, MilliporeSigma, 1:100), respectively, overnight at 4°C. Sections were then incubated with secondary antibodies directed against the primary antibodies for collagen type VI (28903, Rockland, Pottstown, PA, 1:1,000), perlecan (A11006, Invitrogen, Carlsbad, CA, 1:1,000), biglycan and aggrecan (RE234142, Invitrogen, 1:1,000), respectively, for 1hr at room temperature. Finally, samples were counter-stained with DAPI Fluoromount-G (0100-20, SouthernBiotech, Birmingham, AL) prior to imaging. For all the staining, internal negative controls were prepared following the same procedures but without the incubation of primary antibodies. To ensure consistency, all the images were taken on the sections from the center, load-bearing region of the medial tibial plateau (sections #10-30 cut from the medial to lateral ends, after the first 300 µm thickness being trimmed at the medial end). Fluorescence images were taken using an Olympus FV1000 laser scanning microscope (Olympus, Center Valley, PA) with a 488 nm laser at 50% power and 300 ms exposure time in a 16-bit, 1024 × 1024 imaging array format.

2.3. Cryo-sectioning of fresh murine knee joints

Presence of matrix elements does not necessarily indicate that structural integrity or function has been preserved. This is best illustrated by our recent work showing that, at the tissue level, cartilage mechanics in the murine DMM model changes well before histological evidences of disease are apparent [28]. Exploration of murine tissue mechanics, and micromechanics has, until recently, been a challenge, especially for adult mice [32], due to difficulties in sectioning un-demineralized joint tissues. Here, we overcame this challenge by producing flat cryo-sections from fresh, unfixed murine knees, via the Kawamoto's film-assisted method [33]. In brief, immediately following euthanasia, tibial condyles from both the DMM and Sham knees were dissected and embedded in the optimal cutting temperature (OCT) media ($n = 6$ at 3 days post-surgery, and $n = 4$ at each of the other time points). Cryo-sectioning was applied to first trim ≈ 300 μm of the sample at the medial end, and then, consecutively cut 30 sagittal sections from the medial to lateral ends at ≈ 6 μm thickness with a disposable high-profile microtome blade (DT554S50, C.L. Strukey, Lebanon, PA). During cutting, the block surface with the sample exposed was then covered with a Kawamoto's film (Section-Lab, Hiroshima, Japan), and the blade was inserted under the film to produce unfixed sagittal sections adhered to the overlying film (Fig. 2a). The opposite side of the film was then adhered to a glass coverslip using chitosan-based glue for subsequent AFM tests.

2.4. Immunofluorescence (IF)-guided AFM nanomechanical mapping

Following established procedures [34], cryo-sections were labelled by immunofluorescent antibodies specific for collagen VI, a marker of cartilage PCM [9]. Sections were first blocked in 10% goat serum (178144A, Life Technologies, Carlsbad, CA) diluted in assay buffer (0.1% BSA, Invitrogen) in 1 × PBS, and then incubated with primary antibody for collagen VI (70R-CR009X, Fitzgerald, 1:50 dilution) in 10% goat serum, each for 20 minutes at room temperature. Next, sections were washed with 1 × PBS twice for 5 minutes, and then, incubated in a dark room with the secondary antibody (goat anti-rabbit IgG, Lot 28903, Rockland) for 20 minutes. Finally, samples were washed twice with 1 × PBS for 5 minutes, and tested using a Molecular Force Probe-3D AFM (MFP-3D, Asylum Research, Goleta, CA) integrated with a Cascade II EMCCD camera and a dual-view filter (Photometrics, Tucson, AZ) for total internal reflectance fluorescence (TIRF) microscopy. During the test, fluorescence images were obtained simultaneously with a 488 nm laser at 40% power in a 16-bit, 512 × 512 imaging array format.

For each joint, two to three sections were chosen from the central, load-bearing region of the tibial cartilage that is in direct contact with condylar cartilage during joint loading (sections #10-30 cut from the medial to lateral ends, following trimming of the first 300 µm thickness at the medial end). On each section, one to two regions of interest (ROIs) were identified in the middle/deep zone of uncalcified cartilage layer, ≈ 20-40 µm from the tibia surface (Fig. 2a). Each ROI had a size of 20 × 20 μm^2, and contained 1-2 well-defined ring-shape PCM terrains. Within each ROI, AFM nanomechanical mapping was performed in a 40 × 40 grid (1,600 indents) using polystyrene microspherical tips ($R \approx 2.25$ μm, nominal $k \approx 0.6$ N/m, HQ:NSC36/tipless/Cr-Au, cantilever C, NanoAndMore, Watsonville, CA) up to ≈ 100 nN maximum indentation force at 10 μm/s effective indentation depth rate [35]. For each indentation, the effective indentation modulus, E_{ind}, was calculated by fitting the entire loading portion of each indentation force-depth (F-D) curve to the finite thickness-corrected Hertz model (Fig. 2b) [36]. The modulus of Kawamoto's film was measured to be ≈ 17.0 ± 4.2 MPa (≥ 10 locations on 3 samples), which is > 10 × higher than that of cartilage, and thus, was assumed to be infinite in the model. Throughout the experiment, sections were immersed in PBS with protease inhibitors (Pierce 88226, ThermoFisher, Waltham, MA) to minimize post-mortem degradation. Next, using the corresponding IF image of collagen VI, we partitioned each map into three distinct domains: the PCM, T/IT-ECM, and the domain corresponding to cell remnants (e.g., cellular debris consisting of cytoplasmic organelles and nucleus damaged during sectioning) using a custom MATLAB (MathWorks, Natick, MA) code. We then analyzed the moduli of PCM and T/IT-ECM separately and excluded values corresponding to cell remnants (Fig. 2c,d).

To test if the cryo-sectioning procedure and associated freezing-thawing cycle alter tissue micromechanics, we compared the modulus of the T/IT-ECM with the cartilage modulus measured on condyle surfaces via classical AFM-nanoindentation from our previous work [28], both from the Sham joints at the 2-week time point (Fig. 2e). We did not detect significant differences between the two groups, indicating that the sample processing procedure did not significantly alter the micromechanics of cartilage matrix. It is worth noting that, the average micromodulus of the entire map without partitioning is significantly lower than that of the T/IT-ECM or the whole tissue, which can be attributed to the inclusion of lower moduli measured on the PCM and cell remnants.

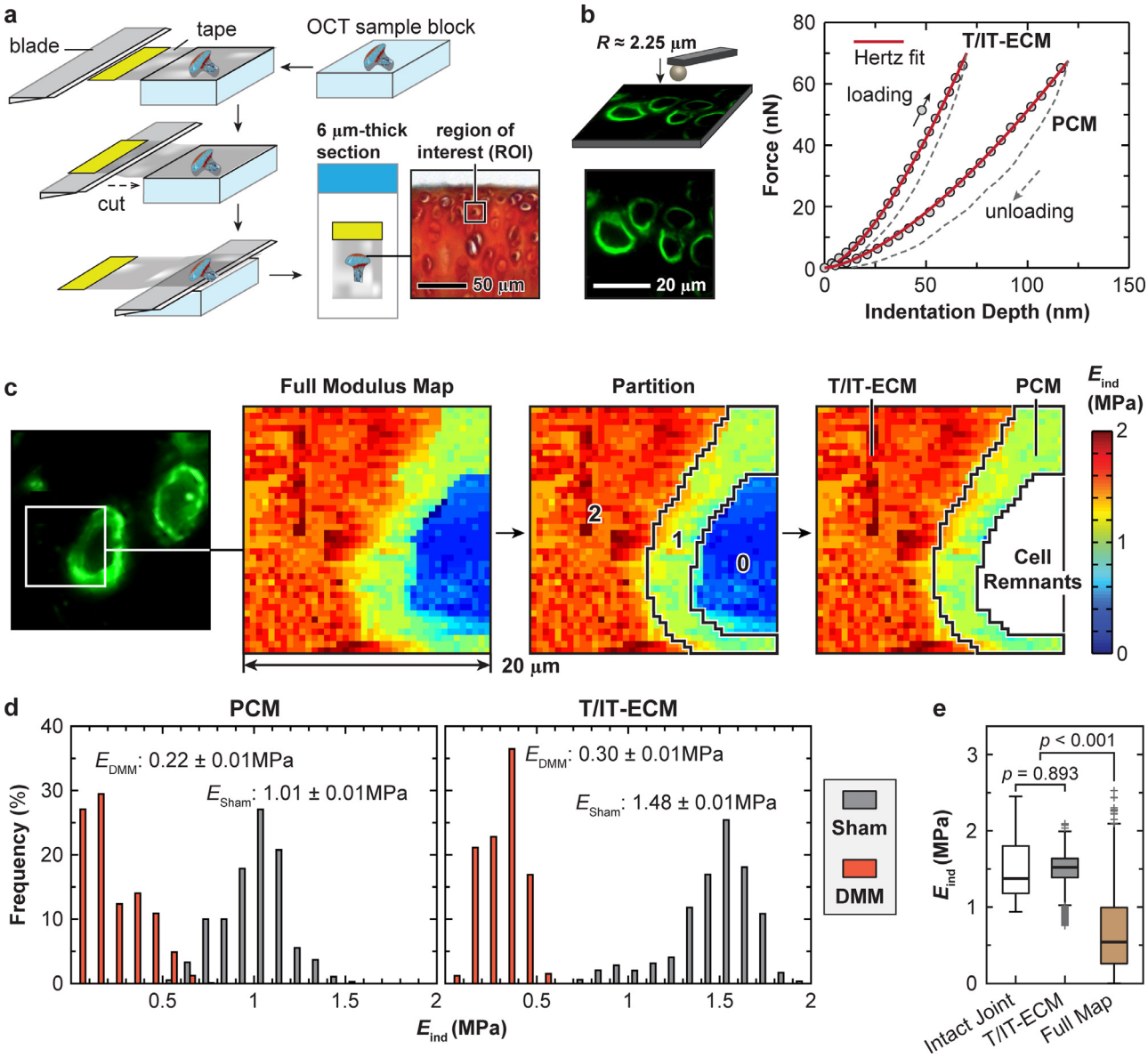

Fig. 2. **a)** Schematic illustration of the Kawamoto's film-assisted cryo-sectioning for the preparation of ≈ 6-μm-thick, unfixed sagittal sections of murine knee articular cartilage integrated with the subchondral bone. Shown together is the representative region of interest (ROI) identified in the middle/deep layer of uncalcified cartilage from the central, load-bearing region of tibial cartilage. **b)** Left panel: Schematic illustration of immunofluorescence (IF)-guided AFM nanomechanical mapping on murine cartilage cryo-section using a microspherical tip ($R \approx 2.25$ μm); the PCM is immunolabeled with collagen VI. Right panel: Two representative indentation force versus depth (*F-D*) curves obtained on the cryo-section from one Sham joint (measured in PBS, 10 μm/s rate), solid line: finite thickness-corrected Hertz model fit to the entire loading portion of the *F-D* curve. **c)** Representative indentation modulus map with corresponding collagen VI IF image of the Sham joint. Based on the IF image, the map was partitioned into three domains: PCM (region 1), T/IT-ECM (region 2) and cell remnants (region 0) to enable the separation of PCM and T/IT-ECM moduli, and the removal of artifacts measured from cell remnants. **d)** Distribution of indentation modulus, E_{ind}, of T/IT-ECM and PCM at all indentation locations (> 600 locations per group, $n = 4$ joints), for the Sham and DMM groups. **e)** Comparison of moduli measured from the intact condyle cartilage surface (adapted from [28]), T/IT-ECM and unpartitioned full map from the Sham joints. Results shown in panels b)-e) are obtained from the joints at 2 weeks post-surgery.

2.5. Intracellular $[Ca^{2+}]_i$ signaling under osmotic stimulation

To evaluate how chondrocyte mechanotransduction changed during PTOA progression, we studied chondrocyte intracellular calcium signaling, $[Ca^{2+}]_i$. Because chondrocytes sense both their physical environment and additionally respond to superimposed mechanical deformations [37], we also queried chondrocyte $[Ca^{2+}]_i$ response to physical perturbation. Limited by the small dimension and irregular shape of murine joints, we were unable to directly apply well-defined compressive strains. Instead, we applied osmotic stimuli by altering the ionic strength from isotonic to hypotonic Dulbecco's Modified Eagle Medium (DMEM) conditions [38]. At each time point, for additional mice ($n = 4$), we labeled cells within the tibia with intracellular calcium indicator Ca-520™ AM (15 μM, AAT Bioquest, Sunnyvale, CA) in isotonic DMEM at 37°C for 1 hr, and then, gently washed three times with DMEM. Time-series of confocal images were taken at 37°C on the same group of cells every 2 seconds for up to 15 min with a 20 × objective (LSM700, Zeiss, Oberkochen, Germany) in both isotonic (330 mOsm, ionic strength (IS) = 0.15M) and hypotonic (165 mOsm, IS = 0.075 M) DMEM with protease inhibitors (Pierce 88266, ThermoFisher). For each time point and IS condition, 50-60 chondrocytes in each sample were analyzed, following established procedures [39]. The pattern of $[Ca^{2+}]_i$ oscillation in each cell was characterized by the intensity of the fluorescent signal and its transient behavior. A responsive cell was considered as any cell

Table 1
Summary of averaged values and statistical analysis outcomes between the Sham and DMM knees from 3 days to 8 weeks post-surgery, shown as mean ± 95% CI from values averaged by animals for E_{ind}, and by cells for $[Ca^{2+}]_i$ parameters

E_{ind} (MPa)	PCM				T/IT-ECM			
	3 days	1 week	2 weeks	8 weeks	3 days	1 week	2 weeks	8 weeks
Sham	0.91 ± 0.09	1.06 ± 0.07	1.03 ± 0.19	1.03 ± 0.05	1.52 ± 0.15	1.48 ± 0.62	1.49 ± 0.22	1.54 ± 0.21
DMM	0.79 ± 0.08	0.44 ± 0.20	0.15 ± 0.20	0.13 ± 0.04	1.41 ± 0.12	0.56 ± 0.16	0.28 ± 0.14	0.33 ± 0.07
p-value	0.016	0.015	0.004	< 0.0001	0.248	0.044	0.005	0.001
$\%R_{cell}$	Isotonic				Hypotonic			
	3 days	1 week	2 weeks	8 weeks	3 days	1 week	2 weeks	8 weeks
Sham	57 ± 11	62 ± 10	66 ± 12	70 ± 12	88 ± 8	83 ± 10	82 ± 10	84 ± 10
DMM	55 ± 11	35 ± 8	16 ± 4	14 ± 4	69 ± 11	58 ± 11	41 ± 9	37 ± 8
p-value	0.774	< 0.001	< 0.0001	< 0.0001	0.015	0.005	< 0.0001	< 0.0001
n_{peak}	Isotonic				Hypotonic			
	3 days	1 week	2 weeks	8 weeks	3 days	1 week	2 weeks	8 weeks
Sham	4.30 ± 0.37	3.94 ± 0.20	4.00 ± 0.23	4.12 ± 0.18	6.45 ± 0.48	6.66 ± 0.35	6.90 ± 0.46	7.00 ± 0.36
DMM	3.83 ± 0.25	2.69 ± 0.20	1.76 ± 0.23	1.52 ± 0.15	4.26 ± 0.20	3.04 ± 0.24	1.96 ± 0.16	1.70 ± 0.14
p-value	0.251	0.002	< 0.0001	< 0.0001	0.002	< 0.0001	< 0.0001	< 0.0001
t_{peak}(sec)	Isotonic				Hypotonic			
	3 days	1 week	2 weeks	8 weeks	3 days	1 week	2 weeks	8 weeks
Sham	40.0 ± 0.7	39.0 ± 0.6	40.3 ± 0.9	38.9 ± 1.0	20.2 ± 0.5	21.2 ± 0.6	23.4 ± 1.0	22.9 ± 0.9
DMM	43.2 ± 1.0	52.7 ± 1.2	68.4 ± 3.4	82.1 ± 2.2	28.8 ± 0.7	42.6 ± 0.8	60.8 ± 2.4	73.8 ± 1.6
p-value	0.021	< 0.0001	0.005	< 0.0001	< 0.0001	< 0.0001	< 0.0001	< 0.0001

Table 2
Summary of statistical analysis outcomes of comparisons across the time points for each surgery type

Time Points	E_{ind}				$\%R_{cell}$			
	Sham		DMM		Sham		DMM	
	PCM	T/IT-ECM	PCM	T/IT-ECM	Iso.	Hypo.	Iso.	Hypo.
3 days vs 1 week	0.089	0.974	< 0.0001	< 0.0001	0.742	0.767	0.018	0.499
3 days vs 2 weeks	(not	(not	< 0.0001	< 0.0001	(not	(not	< 0.0001	0.001
3 days vs 8 weeks	sig.)	sig.)	< 0.0001	< 0.0001	sig.)	sig.)	< 0.0001	< 0.001
1 week vs 2 weeks			< 0.001	< 0.001			< 0.001	0.078
1 week vs 8 weeks			< 0.0001	0.004			< 0.0001	0.012
2 weeks vs 8 weeks			0.990	0.907			0.945	0.879
Time Points	n_{peak}				t_{peak}			
	Sham		DMM		Sham		DMM	
	Iso.	Hypo.	Iso.	Hypo.	Iso.	Hypo.	Iso.	Hypo.
3 days vs 1 week	0.825	1.000	0.012	0.009	0.289	0.660	0.008	< 0.0001
3 days vs 2 weeks	(not	(not	< 0.0001	< 0.0001	(not	0.015	< 0.0001	< 0.0001
3 days vs 8 weeks	sig.)	sig.)	< 0.0001	< 0.0001	sig.)	0.044	< 0.0001	< 0.0001
1 week vs 2 weeks			0.018	0.004		0.107	< 0.001	< 0.0001
1 week vs 8 weeks			< 0.001	< 0.001		0.283	< 0.0001	< 0.0001
2 weeks vs 8 weeks			0.835	0.785		0.928	< 0.001	< 0.0001

in which the magnitude of the peak signal exceeded four times the maximum fluctuation of the baseline signal. The responsive rate, $\%R_{cell}$, at each time point for each condition was calculated by determining the fraction of responsive cells relative to the total cell number within a region of interest. For every cell that was responsive, the total number of $[Ca^{2+}]_i$ peaks, n_{peak}, was counted during the 15 minute observation period, and the average duration of peaks from each responding cell, t_{peak}, was extracted from the $[Ca^{2+}]_i$ transient.

2.6. Blocking of catabolic enzymatic activities in vivo

To test whether altered PCM micromechanics was causal with respect to changes in chondrocyte mechanosensing, we carried out a study to systemically block matrix remodeling post-injury via GM6001, a hydroxamate zinc-chelating active site-directed enzyme inhibitor, which blocks the activities of a broad spectrum of matrix metallopeptidases (MMPs) and also reduces aggrecanase activities to slow down matrix degradation [40]. Following our established procedure [28], we performed daily intraperitoneal injection of 4 mg/kg/day GM6001 (sc-203979, Santa Cruz Biotech) starting from one day before surgery, following our established procedure [28]. For the control group, the same amount of vehicle dimethyl sulfoxide (DMSO, BP231-100, ThermoFisher) was intraperitoneally injected, starting from one day before surgery ($n = 7$). Animals were sacrificed at one week after surgery for IF-AFM ($n = 4$) and chondrocyte $[Ca^{2+}]_i$ signaling tests ($n = 3$), respectively.

2.7. Statistical analysis

Linear statistical models were applied for analyzing all the quantitative outcomes using the R package lme4 (version 1.1-19) [41]. For continuous dependent variables including E_{ind} and t_{peak}, the linear mixed effect model was applied. For non-continuous variables, the generalized linear model was applied to n_{peak} (count) with the Poisson family, and to $\%R_{cell}$ (binary) with the binomial

Table 3
Summary of averaged values and statistical analysis outcomes between the Sham and DMM knees under the vehicle or GM6001 treatment, shown as mean ± 95% CI from values averaged by animals for E_{ind}, and by cells for $[Ca^{2+}]_i$ parameters

E_{ind} (MPa)	PCM			T/IT-ECM		
	Vehicle	GM6001	*p*-value	Vehicle	GM6001	*p*-value
Sham	0.98 ± 0.08	1.02 ± 0.13	0.380	1.43 ± 0.13	1.55 ± 0.16	0.242
DMM	0.37 ± 0.08	0.74 ± 0.13	< 0.001	0.61 ± 0.06	1.01 ± 0.14	< 0.001
p-value	< 0.0001	0.003		< 0.0001	< 0.001	
$\%R_{cell}$	Isotonic			Hypotonic		
	Vehicle	GM6001	*p*-value	Vehicle	GM6001	*p*-value
Sham	59 ± 9	63 ± 10	1.000	72 ± 10	68 ± 10	0.640
DMM	32 ± 6	46 ± 8	0.035	36 ± 7	56 ± 9	0.009
p-value	< 0.001	0.021		< 0.001	0.058	
n_{peak}	Isotonic			Hypotonic		
	Vehicle	GM6001	*p*-value	Vehicle	GM6001	*p*-value
Sham	3.32 ± 0.17	3.11 ± 0.17	1.000	4.78 ± 0.19	4.77 ± 0.20	0.982
DMM	2.06 ± 0.17	2.44 ± 0.16	0.626	3.00 ± 0.20	3.30 ± 0.19	1.000
p-value	0.002	0.026		0.002	0.002	
t_{peak} (sec)	Isotonic			Hypotonic		
	Vehicle	GM6001	*p*-value	Vehicle	GM6001	*p*-value
Sham	29.7 ± 1.8	28.3 ± 1.0	0.620	23.0 ± 0.7	22.3 ± 0.6	0.362
DMM	54.1 ± 1.6	39.1 ± 1.3	0.004	42.1 ± 1.2	30.2 ± 1.0	0.004
p-value	0.006	< 0.0001		0.004	< 0.0001	

family, respectively. This is because for non-continuous dependent variables, it is inappropriate to assume error normality, which is required by the linear model. In these tests, surgery type (DMM versus Sham), time points (3 days to 8 weeks), treatment type (vehicle versus GM6001), tissue region (PCM versus T/IT-ECM) and osmolarity condition (hypo- versus isotonic) were treated as fixed effect factors when applicable, with interaction terms between surgery and time point, or between surgery and treatment type, while the individual animal effect was treated as a randomized factor. Prior to the test, likelihood ratio test was applied to the data to determine the choice of two covariance structures, unstructured versus compound symmetry. For all the variables, we found significant interactions between surgery type and time point ($p < 0.01$), and between surgery type and treatment type ($p < 0.01$, except for $\%R_{cell}$, $p = 0.014$ and not significant for n_{peak}, $p = 0.128$). Therefore, Holm-Bonferroni family-wise error correction was applied to adjust for multiple contrasts when testing the effect of surgery at each time point or for each treatment type, or the effect of treatment for each surgery type, in which, each region or osmolarity condition was analyzed separately. Within each surgery type, if there is a significant effect among the four time points, Tukey-Kramer post-doc multiple comparison was applied to perform pair-wise comparisons between the time points. For all the parameters, the effect of tissue region ($p < 0.001$) and osmolarity ($p < 0.001$, except for $\%R_{cell}$, $p = 0.012$, and for t_{peak}, $p = 0.001$, both in the treatment study) were always found to be significant, regardless of time point, surgery type or treatment type. Key statistical outcomes on the effects of surgery type, time points and treatment were summarized in Tables 1-3. In all the tests, the significance level was set at $\alpha = 0.05$, and all the *p*-values have been adjusted for family-wise type I errors.

3. Results

3.1. Distribution of PCM biomolecules in the DMM model

In healthy cartilage, the PCM has distinct composition and structure relative to the T/IT-ECM (Fig. 1a). For the Sham group, as expected [9], collagen VI, perlecan and biglycan were localized in the PCM, while aggrecan was present throughout the matrix but more concentrated in the PCM (Fig. 1b). For the DMM group, at 8 weeks, collagen VI, perlecan and biglycan remained to be localized in the PCM. For aggrecan, there was a reduction in staining, which is consistent with literature showing decrease of sulfated glycosaminoglycans (sGAGs) in this model [26]. However, aggrecan remained to be preferentially concentrated in the PCM. Based on these observations, it appeared that the PCM did not lose its compositional or morphological distinction with respect to the T/IT-ECM by 8 weeks after DMM. Thus, the DMM model serves as a valid in vivo model for elucidating the changes of PCM micromechanobiology in the initiation and progression of PTOA over the testing time frame.

3.2. Early reduction of the PCM micromodulus after DMM

Applying the Kawamoto's film-assisted cryo-sectioning [33] and IF-AFM nanomechanical mapping (Fig. 2a), we directly quantified the micromodulus of the PCM and T/IT-ECM (Fig. 3). For both Sham and DMM knees, the modulus, E_{ind}, of the PCM was significantly lower than that of the T/IT-ECM for all groups (Fig. 3, $p < 0.001$), consistent with the literature reporting lower PCM modulus in both healthy and OA cartilage [24, 32, 35]. Between the two surgery groups, as early as 3 days post-surgery, the PCM of the DMM joints exhibited a moderate, but significant modulus reduction (0.91 ± 0.09 MPa versus 0.78 ± 0.08 MPa for Sham and DMM, respectively, a 14 ± 6% reduction, mean ± 95% CI of the averaged E_{ind} values from $n = 6$ animals, $p = 0.016$, see Table 1). These results indicate that degradation of the PCM began very soon after DMM. This modulus reduction became further aggravated during the progression of OA, reaching 58 ± 21%, 86 ± 11% and 87 ± 3% by 1, 2 and 8 weeks after DMM, respectively (Fig. 3b, Table 1).

In comparison to the PCM, the modulus of the T/IT-ECM did not show a significant reduction at 3 days post-surgery (1.52 ± 0.14 MPa versus 1.40 ± 0.12 MPa for Sham and DMM, or a 7 ± 13% change, $p = 0.248$, Table 1). However, by 1 week post-DMM, the T/IT-ECM modulus also started to show significant reduction (60 ±

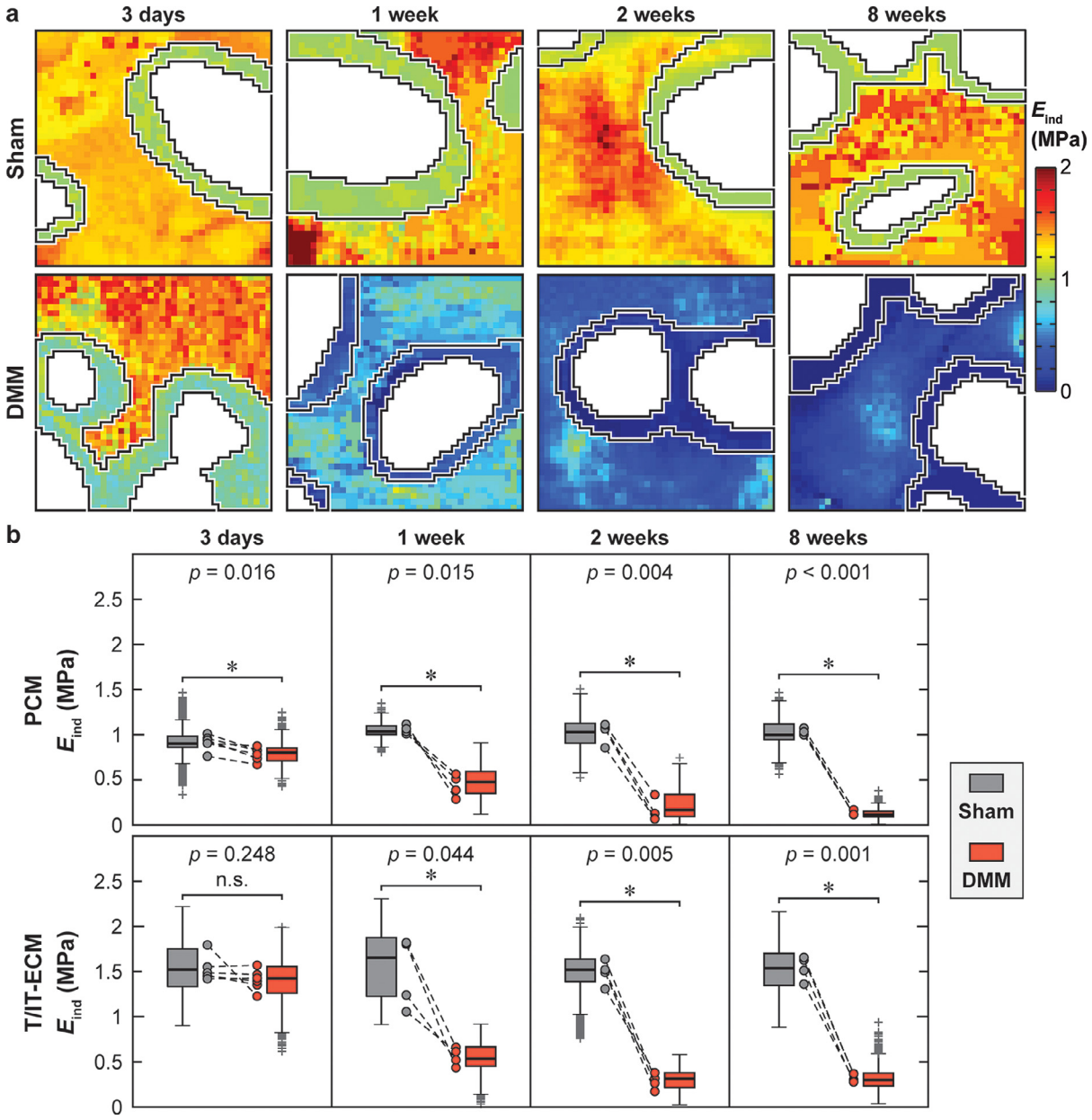

Fig. 3. a) Representative indentation modulus maps of the PCM and T/IT-ECM partitioned for the Sham and DMM cartilage at 3 days and 1, 2 and 8 weeks post-surgery. Moduli corresponding to cell remnants were removed (white voids). **b)** Box-and-whiskers plots of the PCM and T/IT-ECM micromodulus for the Sham versus DMM cartilage at each time point (> 600 locations for each region, $n = 4$ animals at each time point, except for $n = 6$ at the 3-day time point). Each matched pair of circles represents the average modulus of one DMM knee and its contralateral Sham knee, *: $p < 0.05$ between Sham and DMM surgeries from the averaged modulus of each joint (n.s.: not significant). See Tables 1 and 2 for the complete list of adjusted p-values.

22%), which became more substantial by 2 weeks (80 ± 12%) and 8 weeks (79 ± 3%) (Fig. 3b, Table 1). Furthermore, starting at the 1-week time point, the degree of modulus reduction was comparable for both the PCM and T/IT-ECM. Therefore, in both regions, we noted a significant trend of progressive modulus decrease from 3 days to 8 weeks (Table 2). In contrast, for the Sham group, the modulus remained unchanged throughout the testing time frame in both the PCM and T/IT-ECM (Table 2).

3.3. Altered chondrocyte $[Ca^{2+}]_i$ responses to osmotic stimuli after DMM

For all groups, we observed spontaneous $[Ca^{2+}]_i$ oscillations (Fig. 4a,b). In isotonic DMEM, the temporal parameters, including $\%R_{cell}$, n_{peak} and t_{peak}, all remained consistent throughout the 3-day to 8-week period for the Sham group (Fig. 4c-e, Table 2). Comparing the Sham and DMM groups, we did not observe significant differences in $[Ca^{2+}]_i$ activities at 3 days post-surgery, aside from a slight increase in t_{peak} (Fig. 4c-e, Table 1). Strikingly, though, starting at the 1-week time point, the DMM group showed significantly decreased $\%R_{cell}$ and n_{peak}, as well as increased t_{peak} (Fig. 4c-e, Table 1). As the OA development advanced, the contrast between the DMM and Sham groups became progressively more pronounced. Under hypo-osmotic stimuli, for both surgery groups, chondrocytes $[Ca^{2+}]_i$ responses were significantly enhanced compared to the isotonic condition, as marked by increased $\%R_{cell}$, n_{peak} and shorter t_{peak} ($p < 0.0001$). For the Sham group, similar to those observed in isotonic DMEM, cell responses remained consistent throughout the 3-day to 8-week period, except for a slight change in t_{peak} (Fig. 4c, Table 2). For the DMM group, however,

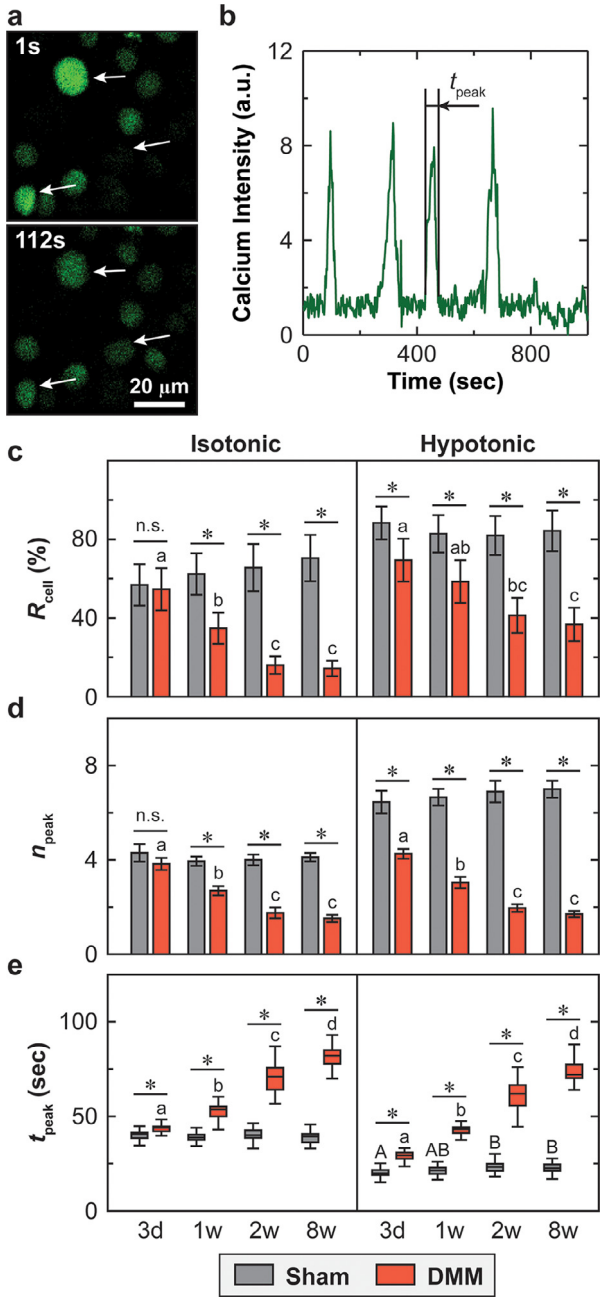

Fig. 4. a) Representative confocal images of murine chondrocyte $[Ca^{2+}]_i$ signaling at the baseline and with hypo-osmotic challenge. Chondrocytes were labeled with Ca-520™ AM and time series images were recorded using a confocal microscope with a 20 × objective submerged in DMEM at 37°C. **b)** Representative $[Ca^{2+}]_i$ oscillation intensity curve of a single cell over a 15-min time frame illustrating the definition of t_{peak}, the duration of each peak. **c-e)** Comparison of $[Ca^{2+}]_i$ signaling characteristics between Sham and DMM groups at each time point and osmolarity: c) percentage of responding cells, $\%R_{cell}$ (mean ± 95% CI), d) number of peaks within the 15-min testing time frame, n_{peak} (mean ± 95% CI), e) duration of each peak, t_{peak} (box plot, outliers are not shown to increase clarity). Data represent ≥ 60 responding cells pooled from $n = 4$ animals for each group. *: $p < 0.05$ between Sham and DMM groups. For longitudinal comparisons, for the Sham group, there was no significant difference among all four time points, except for t_{peak} in the hypotonic condition. Different letters indicate significant differences between time points (n.s.: not significant). See Tables 1 and 2 for the complete list of adjusted *p*-values.

as early as 3 days post-surgery, the elevated $[Ca^{2+}]_i$ responses to hypo-osmotic stimuli were significantly reduced compared to the Sham group, marked by lower $\%R_{cell}$, n_{peak} and longer t_{peak}. At later time points, such reduction became progressively more substantial (Fig. 4c-e, Table 1). Furthermore, within the DMM group, $[Ca^{2+}]_i$ responses also became increasingly suppressed with the progression of OA from the 3-day to 8-week period (Fig. 4c-e, Table 2).

3.4. Blocking early proteolytic degradation of the PCM preserves PCM micromechanobiology

With the administration of GM6001, the inhibitor of MMP and aggrecanase activities, the micromodulus of PCM in the DMM knees (0.74 ± 0.13 MPa) was significantly elevated compared to the vehicle control group subjected to DMM (0.37 ± 0.08 MPa, $p < 0.001$, Fig. 5a). Thus, although the PCM micromodulus in the DMM knees was still reduced compared to the Sham knees with GM6001 (28 ± 18% reduction, $p = 0.003$), the degree of reduction was much less than that of the vehicle group (62 ± 10%, $p < 0.001$). A similar rescue effect was detected for the T/IT-ECM micromodulus of the DMM knees, but no significant differences were observed for the Sham knees (Fig. 5a, Table 3). In the DMM knees, when the matrix degradation was partially blocked, chondrocyte $[Ca^{2+}]_i$ activities were also restored towards baseline levels, as signified by the higher $\%R_{cell}$ and shorter t_{peak}, in both hypotonic and isotonic DMEM, although no significant changes were noted for n_{peak}. In the Sham knees, as expected, there were not changes in chondrocyte $[Ca^{2+}]_i$ activities with GM6001 (Fig. 5b, Table 3). In our previous study, we have shown that GM6001 significantly attenuated the activities of MMPs in the mouse joints using MMPSense™ 645 [28], these altered $[Ca^{2+}]_i$ transients can be attributed to the restoration of the micromechanical properties of cartilage matrix due to attenuated catabolism, and in particular, the immediate cell microenvironment, i.e., the PCM. These data indicate that retaining the integrity of the PCM can effectively protect the normal mechanosensitive activities of chondrocytes, potentially improving the maintenance of joint health.

4. Discussion

4.1. Micromodulus of the PCM is a sensitive indicator of OA initiation

This study reveals that alteration of the PCM, the immediate cell microenvironment, is one of the earliest events seen upon the initiation of PTOA. Here, the reduction of PCM modulus (3 days after DMM) precedes changes in cartilage biomechanics in the further-removed T/IT-ECM (Fig. 2) and at the tissue level (1 week after) [28], as well as any appreciable morphological changes of cartilage detectable by conventional histology (4-8 weeks after) [26]. In comparison to the cartilage bulk ECM, the PCM has a higher concentration of proteoglycans (Fig. 1), and has a faster turnover rate [21]. Matrix biomolecules in this region are thus highly susceptible to catabolic enzymatic degradation [42]. In fact, aggrecan is one of the first molecular constituents that undergo enzymatic fragmentation upon OA initiation [23]. Owing to the immediacy of cell-PCM contact, fragmentation of aggrecan in early OA is largely localized to the pericellular domain, as illustrated by our recent work on the aggrecan degradation neoepitope staining, VDIPEN^{341} at 2 weeks after DMM (Fig. 6a [28]) and the literature [42]. Under the IF-AFM, indentation with a microspherical indenter tip of $R \approx 2.25$ μm and a maximum depth of $D_{max} \approx 0.5$ μm yields a ≈ 1.4 μm effective tip-sample contact radius, or ≈ 6.3 μm^2 contact area. Given that each aggrecan molecule consists of ≈ 400 nm-long core protein decorated with ≈ 40 nm-long chondroitin sulfate (CS)-GAG side chains [43], the micromodulus

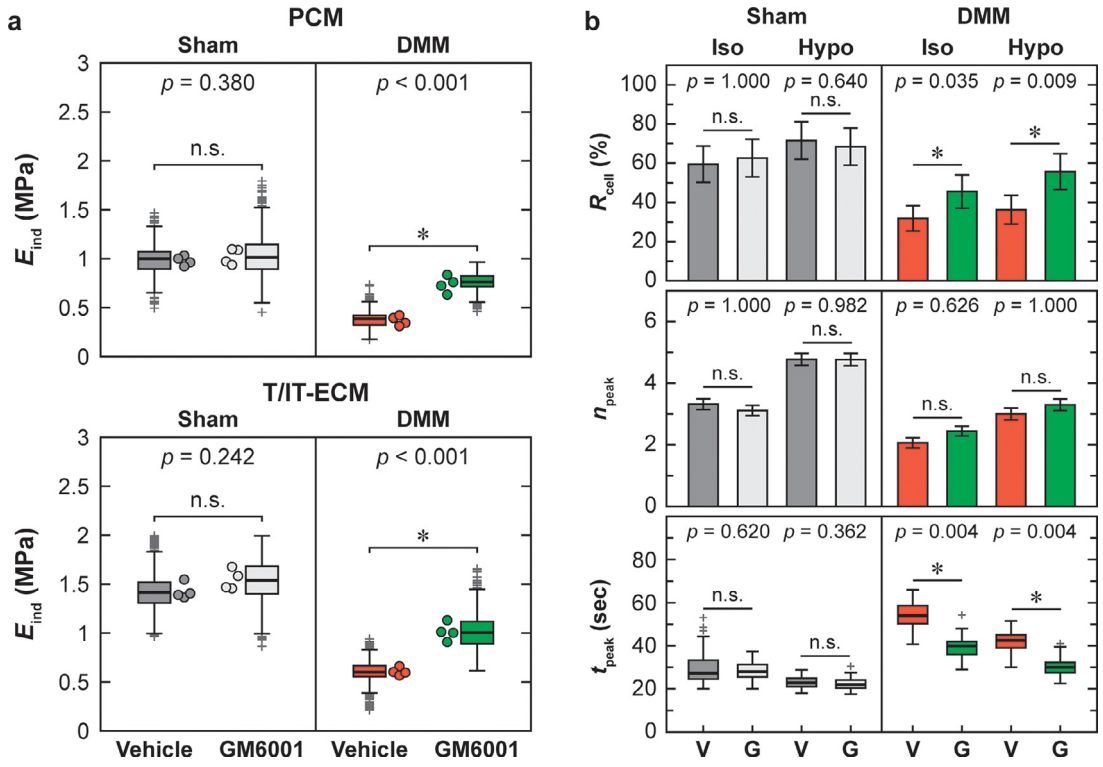

Fig. 5. a) Comparison of the PCM and T/IT-ECM micromodulus for Sham and DMM cartilage in vehicle and GM6001-treated joints at 1 week post-surgery (> 600 locations for each region, $n = 4$ animals at each time point). Each circle represents the average modulus of one DMM or Sham knee, *: $p < 0.001$ between vehicle and GM6001-treated DMM joints from the averaged modulus of each joint. **b)** Comparison of $[Ca^{2+}]_i$ signaling characteristics between the vehicle (V) and GM6001 (G)-treated joints at 1 week post-surgery in isotonic and hypotonic DMEM: percentage of responding cells, $\%R_{cell}$ (mean ± 95% CI), number of peaks within the 15-min testing timeframe, n_{peak} (mean ± 95% CI), and duration of each peak, t_{peak} (box-and-whisker plot). Data represent responding cells pooled from $n = 3$ animals for each group. *: $p < 0.05$ between vehicle and GM6001 groups (n.s.: not significant). See Table 3 for the complete list of adjusted p-values.

of the PCM reflects the local integrity of a few aggrecan molecules, collagen fibrils (≈ 30-80 diameter [44]) and other minor matrix constituents, and can be highly sensitive to matrix disruption at the molecular level. Therefore, during OA initiation, these subtle molecular changes, which may not yet be directly detectable by conventional imaging or biochemical assays [45], are manifested through the impaired PCM micromechanics (Fig. 3b).

4.2. Comparison of the sensitivity of the PCM and T/IT-ECM to OA initiation

In comparison to the PCM, the T/IT-ECM is more distant to cells, and has a lower concentration of aggrecan and a higher concentration of thicker collagen II/IX/XI heterotypic fibrils [9]. In OA, degradation of collagen fibrils occurs at a later time than that of aggrecan [46]. These factors suggest that the T/IT-ECM is likely to be less sensitive to OA initiation than the PCM. In the DMM model, the reduction of T/IT-ECM micromodulus starts at 1 week after DMM, a similar time frame as the change of tissue-level modulus [28], but slightly delayed compared to that of the PCM. Despite this later start time, the degree of modulus reduction was comparable between these two domains throughout the 1- to 8-week period (Fig. 6c). This high sensitivity of T/IT-ECM micromechanics to OA, and the associated lack of contrast between the PCM and T-IT/ECM, could be attributed to the much higher cell density of murine cartilage (≈ 20% volume ratio in adult tissues) relative to that of larger animals or human (< 5%) [47]. This indicates more efficient cell-cell communications, and means that the T/IT-ECM also resides in the vicinity of cells (furthest distance < 10 μm from cell surface). Furthermore, given the whole organ nature of OA, catabolism can arise from inflammatory cells from other parts of the knee [48]. The MMPs and aggrecanases synthesized by other cells types, such as synovial macrophages, can also contribute to the breakdown of cartilage matrix [49]. In this case, the T/IT-ECM and PCM are likely to have similar susceptibility to these cellular activities. Also, limited by the relatively low biological repeats ($n = 4$ starting at the 1-week time point), it is possible that our test did not detect the subtle differences between the PCM and T/IT-ECM degradation within this period. On the other hand, even by 8 weeks, at this intermediate OA stage, despite this quite substantial modulus reduction throughout the matrix, the PCM has not lost its morphological and compositional distinction from the T/IT-ECM (Fig. 1b). Thus, at this time point, the progression of OA has not reached the clinically-defined advanced OA stage, in which, boundaries between the PCM and T/IT-ECM become less defined, and PCM-specific molecules, such as collagen VI and perlecan, are present throughout the damaged matrix [50, 51]. Collectively, these results underscore that changes in cartilage biomechanics at the microscale precede any gross-level compositional or morphological alterations of cartilage.

4.3. Impact of PCM degradation on chondrocyte mechanotransduction

The impact of PCM degradation on chondrocyte mechanotransduction is highlighted by the altered chondrocyte $[Ca^{2+}]_i$ signaling [52], both at the baseline (isotonic DMEM) and with mechanical challenge (hypotonic DMEM) (Fig. 4). In native cartilage, chondrocyte $[Ca^{2+}]_i$ characteristics are mediated by a multitude of factors, including extracellular [53] and intracellular [54] calcium sources, mechanosensitive ion channels on cell membrane [55, 56], adenosine triphosphate (ATP)-activated intracellular pathways [57] and cell micromechanical environments [38]. In the PCM, negative fixed

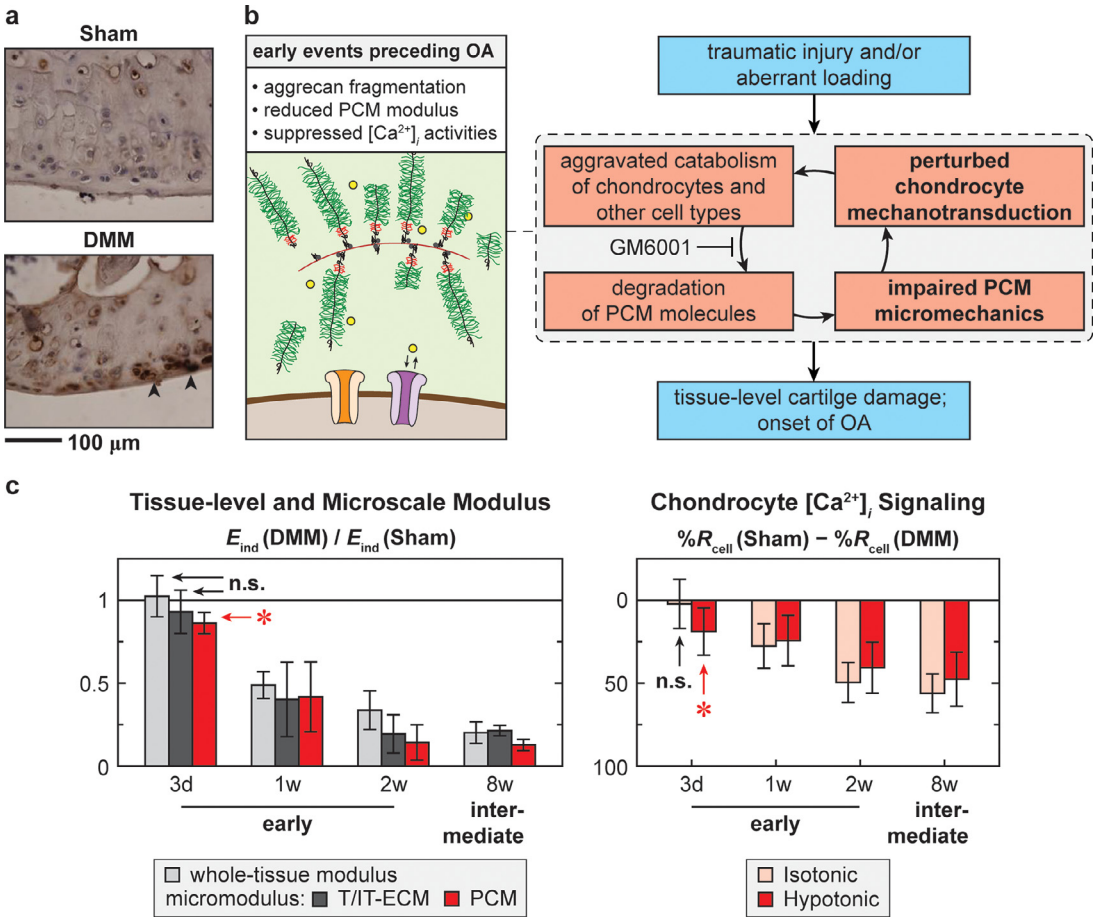

Fig. 6. a) Immunohistochemistry (IHC) staining shows the presence of increased aggrecan degradation neoepitope by MMPs, VDIPEN^{341}, in the pericellular domain (black arrowheads) of medial condyle knee cartilage at 2 weeks after DMM (adapted from Ref. [28] with permission). **b)** Schematic illustration of molecular events taking place in the PCM in early OA, and flow chart showing the feedback loop of molecular and cellular events that contribute to the initiation and progression of OA. **c)** Summary of longitudinal changes in the microscale and tissue-level modulus of cartilage (tissue-level data are adapted from Ref. [28] with permission), and chondrocyte $[Ca^{2+}]_i$ signaling activities, as illustrated by $\%R_{cell}$, in the DMM murine model (mean ± 95% CI, all the bars are significantly different from the baseline, $p < 0.05$, unless noted as "n.s.", i.e., not significant).

charges on proteoglycans function as a reservoir to sequester free counter-ions, thereby providing an important extracellular source of Ca^{2+} (Fig. 1a) [58]. Meanwhile, the osmolarity surrounding the cells is directly determined by these fixed charges in the PCM [59]. Chondrocyte $[Ca^{2+}]_i$ activities are thus expected to be highly sensitive to the integrity of matrix molecules localized in the PCM, especially aggrecan (Fig. 1a). In fact, when aggrecan is degraded in early OA, chondrocyte $[Ca^{2+}]_i$ activities are significantly attenuated as early as 1 week after DMM under baseline (isotonic) conditions (Fig. 4c-e).

Hypo-osmotic stimuli increase the GAG-GAG repulsion within the cartilage matrix [60]. In addition, in hypotonic solutions, isolated chondrocytes undergo a marked volume increase in vitro [61], but such swelling is limited by the stiffer surrounding PCM in situ [18, 61]. Hypotonic stimuli thus increase the compressive strain on both matrix molecules and chondrocyte cells, similar to the effects of applied tissue compression. As expected [38], under the amplified GAG-GAG repulsion, hypotonic stimuli promoted chondrocyte $[Ca^{2+}]_i$ responses, with faster transient characteristics in both Sham and DMM groups (Fig. 4c-e). At 3 days after DMM, although $[Ca^{2+}]_i$ activities were not altered in isotonic (baseline) media, the responses to hypo-osmotic stimuli were significantly attenuated compared to the Sham group (Fig. 4c-e). This could be attributed to the initial degradation of aggrecan in the PCM and the resulting reduction of PCM micromodulus at this early time point (Fig. 2b). In fact, the causal impact of matrix integrity on chondrocyte mechanosensing is highlighted by the rescue effect of the small molecule MMP inhibitor, GM6001 (Fig. 5). When the degradation of the matrix, and in particular, the PCM, is partially blocked by GM6001, chondrocyte $[Ca^{2+}]_i$ activities are also restored toward the baseline level. Meanwhile, the degradation of the T/IT-ECM is also partially rescued (Fig. 5a), so we cannot delineate the influence of the PCM and T/IT-ECM on chondrocyte mechanotransduction. Given the immediacy of PCM-cell contact, blocking PCM degradation could have a more direct impact on restoring chondrocyte mechanotransduction. Thus, these results point to the potential of developing therapeutic strategies using small molecules to stop early aberrant remodeling in this critical cartilage microdomain, i.e., the PCM, to slow or reverse disease progression.

4.4. Implications for human OA

Our findings point to key differences between murine cartilage and those of larger animals or human with regard to matrix microstructure, micromechanics and cell-matrix interactions. Notably, the indentation modulus of healthy, adult murine cartilage PCM (≈ 1 MPa) is about one order of magnitude higher than those of porcine (≈ 60 kPa) [35] or human (≈ 100 kPa) cartilage PCMs [24, 32, 35]. Such contrast is consistent with the reported differences of the tissue-level modulus, where healthy murine cartilage (≈ 1.5 MPa) [28, 62, 63] is also much stiffer than porcine [64], bovine [65] or human [24] cartilage (≈ 0.1-0.5 MPa). These dif-

ferences suggest that the cross-linking and packing of proteoglycans and fibrillar collagens in cartilage matrix are highly variable across species. Also, given that murine cartilage has much higher cell density, there could be substantial differences in the etiology of PTOA between mice and human. Therefore, one limitation of this study is that knowledge gained from the murine DMM model is not directly translatable to human OA. For human cartilage, given its lower cell density, it is possible that the PCM is much more sensitive to OA degeneration compared to the bulk T/IT-ECM. Furthermore, the degeneration characteristics of the PCM and T/IT-ECM could also vary in other forms of OA, such as ageing-associated spontaneous OA, the etiology of which is distinct from the DMM-induced PTOA.

On the technical front, our results underscore the importance of accounting for the microscale heterogeneity when studying highly cellularized tissues. On the murine cartilage section, ratio of the three distinct domains (cells, PCM and T/IT-ECM) is approximately 1:1:3. The domain corresponding to residing chondrocytes consists of cytoplasma and nucleus remnants damaged during cryosectioning. These values do not represent true biophysical characteristics of either cells or matrix, and need to be excluded from data analysis. A blinded indentation mapping does not recognize such heterogeneity or enable the exclusion of confounding artifacts, thereby yielding misleading outcomes. For instance, for Sham cartilage at the 2-week time point, the modulus of T/IT-ECM measured by IF-AFM is similar to that of intact tissue [28], as expected. In contrast, averaging values from the entire modulus map without distinguishing the three domains would yield $>$ 50% lower modulus (Fig. 2e). To this end, IF-guided AFM offers an unbiased tool for quantifying the micromechanics of soft tissues with high cell density and salient structural heterogeneity. On the other hand, the sample preparation for IF-AFM involves cryo-sectioning that disrupts the integrity of whole tissue. Such invasive nature means that application of this method is mainly limited to analyzing post-mortem tissues from animal models or human OA specimens to gain insights of early OA, rather than being used as a diagnostic tool for early OA detection [66].

5. Conclusions

In summary, changes in PCM micromechanobiology are one of the earliest events in OA initiation (Fig. 6b,c). Here, aggravated chondrocyte catabolism leads to local degradation of proteoglycans, especially aggrecan, in the PCM, resulting in reduced micromodulus. This impairs the normal mechanosensing of chondrocytes, contributing to the vicious loop of cartilage degradation in OA (Fig. 6b). The local PCM micromodulus ($E_{\mathrm{ind,\ PCM}}$) and mechanically instigated chondrocyte $[Ca^{2+}]_i$ activity (e.g., $\%R_{\mathrm{cell}}$ in hypotonic DMEM) are two key early indicators of PTOA initiation (Fig. 6c). Furthermore, our data show that attenuating PCM degradation can protect the normal chondrocyte mechanosensing, indicating a potential for preserving joint-wide health, since these local changes precede matrix changes at larger length scales (Fig. 5). This insight, revealed by exploring cell-ECM mechano-crosstalk at the nm-to-μm scale, provides a basis for developing novel strategies for early PTOA detection or intervention by targeting cartilage PCM, and may have impact on other load-bearing diseases as well.

Declaration of interests

The authors declare that they have no known competing financial interests or personal relationships that could have appeared to influence the work reported in this paper.

Acknowledgements

This work was supported by the National Institutes of Health (NIH) Grant AR066824 and AR074490 to LH, the National Science Foundation (NSF) Grant CMMI-1662544 to LH, Drexel Interdisciplinary Collaboration and Research Enterprise (iCARE) for Healthcare by the U.S. Department of Education's Graduate Assistance in Areas of National Need (GAANN) Program to DRC, as well as NIH Grant P30 AR069619 to the Penn Center for Musculoskeletal Disorders (PCMD). The IF-guided AFM nanomechanical mapping via TIRF MFP-3D was carried out at the Singh Center for Nanotechnology at the University of Pennsylvania, part of the National Nanotechnology Coordinated Infrastructure Program, which is supported by the NSF Grant NNCI-1542153.

References

[1] E.M. Roos, Joint injury causes knee osteoarthritis in young adults, Curr. Opin. Rheumatol 17 (2005) 195–200.
[2] F.E. Watt, N. Corp, S.R. Kingsbury, R. Frobell, M. Englund, D.T. Felson, M. Levesque, S. Majumdar, C. Wilson, D.J. Beard, L.S. Lohmander, V.B. Kraus, F. Roemer, P.G. Conaghan, D.J. Mason, Towards prevention of post-traumatic osteoarthritis: report from an international expert working group on considerations for the design and conduct of interventional studies following acute knee injury, Osteoarthritis Cartilage 27 (2019) 23–33.
[3] D.D. Anderson, S. Chubinskaya, F. Guilak, J.A. Martin, T.R. Oegema, S.A. Olson, J.A. Buckwalter, Post-traumatic osteoarthritis: improved understanding and opportunities for early intervention, J, Orthop. Res. 29 (2011) 802–809.
[4] J.H. Kim, G. Lee, Y. Won, M. Lee, J.S. Kwak, C.H. Chun, J.S. Chun, Matrix cross-linking-mediated mechanotransduction promotes posttraumatic osteoarthritis, Proc. Natl. Acad. Sci. U. S. A. 112 (2015) 9424–9429.
[5] R.C. Lawrence, D.T. Felson, C.G. Helmick, L.M. Arnold, H. Choi, R.A. Deyo, S. Gabriel, R. Hirsch, M.C. Hochberg, G.G. Hunder, J.M. Jordan, J.N. Katz, H.M. Kremers, F. Wolfe, for the National Arthritis Data Workgroup, Estimates of the prevalence of arthritis and other rheumatic conditions in the United States, Part II, Arthritis Rheum 58 (2008) 26–35.
[6] C.A. Poole, M.H. Flint, B.W. Beaumont, Chondrons in cartilage: ultrastructural analysis of the pericellular microenvironment in adult human articular cartilages, J. Orthop. Res. 5 (1987) 509–522.
[7] F. Guilak, R.J. Nims, A. Dicks, C.L. Wu, I. Meulenbelt, Osteoarthritis as a disease of the cartilage pericellular matrix, Matrix Biol 71-72 (2018) 40–50.
[8] C. Wang, B.K. Brisson, M. Terajima, Q. Li, K. Hoxha, B. Han, A.M. Goldberg, X.S. Liu, M.S. Marcolongo, M. Enomoto-Iwamoto, M. Yamauchi, S.W. Volk, L. Han, Type III collagen is a key regulator of the collagen fibrillar structure and biomechanics of articular cartilage and meniscus, Matrix Biol 85-86 (2020) 47–67.
[9] R.E. Wilusz, J. Sanchez-Adams, F. Guilak, The structure and function of the pericellular matrix of articular cartilage, Matrix Biol 39 (2014) 25–32.
[10] D. Heinegård, Proteoglycans and more – from molecules to biology, Int. J. Exp. Pathol 90 (2009) 575–586.
[11] T.L. Vincent, C.J. McLean, L.E. Full, D. Peston, J. Saklatvala, FGF-2 is bound to perlecan in the pericellular matrix of articular cartilage, where it acts as a chondrocyte mechanotransducer, Osteoarthritis Cartilage 15 (2007) 752–763.
[12] F. Guilak, A. Ratcliffe, V.C. Mow, Chondrocyte deformation and local tissue strain in articular cartilage: a confocal microscopy study, J. Orthop. Res. 13 (1995) 410–421.
[13] J.B. Choi, I. Youn, L. Cao, H.A. Leddy, C.L. Gilchrist, L.A. Setton, F. Guilak, Zonal changes in the three-dimensional morphology of the chondron under compression: the relationship among cellular, pericellular, and extracellular deformation in articular cartilage, J. Biomech 40 (2007) 2596–2603.
[14] L.G. Alexopoulos, L.A. Setton, F. Guilak, The biomechanical role of the chondrocyte pericellular matrix in articular cartilage, Acta Biomater 1 (2005) 317–325.
[15] B.V. Nguyen, Q. Wang, N.J. Kuiper, A.J. El Haj, C.R. Thomas, Z. Zhang, Strain-dependent viscoelastic behaviour and rupture force of single chondrocytes and chondrons under compression, Biotechnol. Lett 31 (2009) 803–809.
[16] R. Madden, S.K. Han, W. Herzog, Chondrocyte deformation under extreme tissue strain in two regions of the rabbit knee joint, J. Biomech 46 (2013) 554–560.
[17] L.G. Alexopoulos, I. Youn, P. Bonaldo, F. Guilak, Developmental and osteoarthritic changes in Col6a1-knockout mice: biomechanics of type VI collagen in the cartilage pericellular matrix, Arthritis Rheum 60 (2009) 771–779.
[18] N.A. Zelenski, H.A. Leddy, J. Sanchez-Adams, J. Zhang, P. Bonaldo, W. Liedtke, F. Guilak, Type VI collagen regulates pericellular matrix properties, chondrocyte swelling, and mechanotransduction in mouse articular cartilage, Arthritis Rheumatol 67 (2015) 1286–1294.
[19] X. Xu, Z. Li, Y. Leng, C.P. Neu, S. Calve, Knockdown of the pericellular matrix molecule perlecan lowers in situ cell and matrix stiffness in developing cartilage, Dev. Biol 418 (2016) 242–247.
[20] A. Corsi, T. Xu, X.-D. Chen, A. Boyde, J. Liang, M. Mankani, B. Sommer, R.V. Iozzo, I. Eichstetter, P.G. Robey, P. Bianco, M.F. Young, Phenotypic effects of biglycan deficiency are linked to collagen fibril abnormalities, are synergized

by decorin deficiency, and mimic Ehlers-Danlos-like changes in bone and other connective tissues, J. Bone Miner. Res. 17 (2002) 1180–1189.
[21] T.M. Quinn, A.A. Maung, A.J. Grodzinsky, E.B. Hunziker, J.D. Sandy, Physical and biological regulation of proteoglycan turnover around chondrocytes in cartilage explants. Implications for tissue degradation and repair, Ann. N. Y. Acad. Sci. 878 (1999) 420–441.
[22] M.T. Bayliss, S. Howat, C. Davidson, J. Dudhia, The organization of aggrecan in human articular cartilage. Evidence for age-related changes in the rate of aggregation of newly synthesized molecules, J. Biol. Chem. 275 (2000) 6321–6327.
[23] M.W. Lark, E.K. Bayne, L.S. Lohmander, Aggrecan degradation in osteoarthritis and rheumatoid arthritis, Acta Orthop. Scand. Suppl 266 (1995) 92–97.
[24] R.E. Wilusz, S. Zauscher, F. Guilak, Micromechanical mapping of early osteoarthritic changes in the pericellular matrix of human articular cartilage, Osteoarthritis Cartilage 21 (2013) 1895–1903.
[25] M. Danalache, R. Kleinert, J. Schneider, A.L. Erler, M. Schwitalle, R. Riester, F. Traub, U.K. Hofmann, Changes in stiffness and biochemical composition of the pericellular matrix as a function of spatial chondrocyte organisation in osteoarthritic cartilage, Osteoarthritis Cartilage 27 (2019) 823–832.
[26] S.S. Glasson, T.J. Blanchet, E.A. Morris, The surgical destabilization of the medial meniscus (DMM) model of osteoarthritis in the 129/SvEv mouse, Osteoarthritis Cartilage 15 (2007) 1061–1069.
[27] D. Chen, J. Shen, W. Zhao, T. Wang, L. Han, J.L. Hamilton, H.J. Im, Osteoarthritis: toward a comprehensive understanding of pathological mechanism, Bone Res 5 (2017) 16044.
[28] B. Doyran, W. Tong, Q. Li, H. Jia, X. Zhang, C. Chen, M. Enomoto-Iwamoto, X.L. Lu, L. Qin, L. Han, Nanoindentation modulus of murine cartilage: a sensitive indicator of the initiation and progression of post-traumatic osteoarthritis, Osteoarthritis Cartilage 25 (2017) 108–117.
[29] D.E. Clapham, Calcium signaling, Cell 131 (2007) 1047–1058.
[30] Y. Zhou, M. Lv, T. Li, T. Zhang, R. Duncan, L. Wang, X.L. Lu, Spontaneous calcium signaling of cartilage cells: from spatiotemporal features to biophysical modeling, FASEB J 33 (2019) 4675–4687.
[31] E.J. Vanderploeg, C.G. Wilson, S.M. Imler, C.H. Ling, M.E. Levenston, Regional variations in the distribution and colocalization of extracellular matrix proteins in the juvenile bovine meniscus, J. Anat 221 (2012) 174–186.
[32] E.M. Darling, R.E. Wilusz, M.P. Bolognesi, S. Zauscher, F. Guilak, Spatial mapping of the biomechanical properties of the pericellular matrix of articular cartilage measured in situ via atomic force microscopy, Biophys. J 98 (2010) 2848–2856.
[33] T. Kawamoto, K. Kawamoto, Preparation of thin frozen sections from nonfixed and undecalcified hard tissues using Kawamot's film method (2012), Methods Mol. Biol 1130 (2014) 149–164.
[34] I. Youn, J.B. Choi, L. Cao, L.A. Setton, F. Guilak, Zonal variations in the three-dimensional morphology of the chondron measured in situ using confocal microscopy, Osteoarthritis Cartilage 14 (2006) 889–897.
[35] R.E. Wilusz, L.E. DeFrate, F. Guilak, Immunofluorescence-guided atomic force microscopy to measure the micromechanical properties of the pericellular matrix of porcine articular cartilage, J. Royal Soc. Interface 9 (2012) 2997–3007.
[36] E.K. Dimitriadis, F. Horkay, J. Maresca, B. Kachar, R.S. Chadwick, Determination of elastic moduli of thin layers of soft material using the atomic force microscope, Biophys. J 82 (2002) 2798–2810.
[37] F. Guilak, R.A. Zell, G.R. Erickson, D.A. Grande, C.T. Rubin, K.J. McLeod, H.J. Donahue, Mechanically induced calcium waves in articular chondrocytes are inhibited by gadolinium and amiloride, J. Orthop. Res. 17 (1999) 421–429.
[38] Y. Zhou, M.A. David, X. Chen, L.Q. Wan, R.L. Duncan, L. Wang, X.L. Lu, Effects of osmolarity on the spontaneous calcium signaling of in situ juvenile and adult articular chondrocytes, Ann. Biomed. Eng 44 (2016) 1138–1147.
[39] W.M. Han, S.J. Heo, T.P. Driscoll, J.F. Delucca, C.M. McLeod, L.J. Smith, R.L. Duncan, R.L. Mauck, D.M. Elliott, Microstructural heterogeneity directs micromechanics and mechanobiology in native and engineered fibrocartilage, Nat. Mater 15 (2016) 477–484.
[40] E. Nuti, S. Santamaria, F. Casalini, K. Yamamoto, L. Marinelli, V. La Pietra, E. Novellino, E. Orlandini, S. Nencetti, A.M. Marini, S. Salerno, S. Taliani, F. Da Settimo, H. Nagase, A. Rossello, Arylsulfonamide inhibitors of aggrecanases as potential therapeutic agents for osteoarthritis: synthesis and biological evaluation, Eur. J. Med. Chem 62 (2013) 379–394.
[41] D. Bates, M. Mächler, B.M. Bolker, S.C. Walker, Fitting linear mixed-effects models using lme4, J. Stat. Softw 67 (1) (2015) 1–48.
[42] M.G. Chambers, L. Cox, L. Chong, N. Suri, P. Cover, M.T. Bayliss, R.M. Mason, Matrix metalloproteinases and aggrecanases cleave aggrecan in different zones of normal cartilage but colocalize in the development of osteoarthritic lesions in STR/ort mice, Arthritis Rheum 44 (2001) 1455–1465.
[43] L. Han, A.J. Grodzinsky, C. Ortiz, Nanomechanics of the cartilage extracellular matrix, Annu. Rev. Mater. Res 41 (2011) 133–168.
[44] B. Han, Q. Li, C. Wang, P. Patel, S.M. Adams, B. Doyran, H.T. Nia, R. Oftadeh, S. Zhou, C.Y. Li, X.S. Liu, X.L. Lu, M. Enomoto-Iwamoto, L. Qin, R.L. Mauck, R.V. Iozzo, D.E. Birk, L. Han, Decorin regulates the aggrecan network integrity and biomechanical functions of cartilage extracellular matrix, ACS Nano 13 (2019) 11320–11333.
[45] S.P. Ojanen, M.A.J. Finnila, A.E. Reunamo, A.P. Ronkainen, S. Mikkonen, W. Herzog, S. Saarakkala, R.K. Korhonen, Site-specific glycosaminoglycan content is better maintained in the pericellular matrix than the extracellular matrix in early post-traumatic osteoarthritis, PLoS One 13 (2018) e0196203.
[46] M.A. Pratta, W. Yao, C. Decicco, M.D. Tortorella, R.-Q. Liu, R.A. Copeland, R. Magolda, R.C. Newton, J.M. Trzaskos, E.C. Arner, Aggrecan protects cartilage collagen from proteolytic cleavage, J. Biol. Chem. 278 (2003) 45539–45545.
[47] R.A. Stockwell, The interrelationship of cell density and cartilage thickness in mammalian articular cartilage, J. Anat 109 (1971) 411–421.
[48] C.L. Wu, N.S. Harasymowicz, M.A. Klimak, K.H. Collins, F. Guilak, The role of macrophages in osteoarthritis and cartilage repair, Osteoarthritis Cartilage 28 (2020) 544–554, doi:10.1016/j.joca.2019.12.007.
[49] M.J. Wood, A. Leckenby, G. Reynolds, R. Spiering, A.G. Pratt, K.S. Rankin, J.D. Isaacs, M.A. Haniffa, S. Milling, C.M. Hilkens, Macrophage proliferation distinguishes 2 subgroups of knee osteoarthritis patients, JCI Insight 4 (2019) e125325.
[50] F. Tesche, N. Miosge, Perlecan in late stages of osteoarthritis of the human knee joint, Osteoarthritis Cartilage 12 (2004) 852–862.
[51] A.E. Nugent, D.M. Speicher, I. Gradisar, D.L. McBurney, A. Baraga, K.J. Doane, W.E. Horton Jr., Advanced osteoarthritis in humans is associated with altered collagen VI expression and upregulation of ER-stress markers Grp78 and bag-1, J. Histochem. Cytochem. 57 (2009) 923–931.
[52] F. Guilak, D.L. Butler, S.A. Goldstein, F.P. Baaijens, Biomechanics and mechanobiology in functional tissue engineering, J. Biomech 47 (2014) 1933–1940.
[53] B. Pingguan-Murphy, M. El-Azzeh, D.L. Bader, M.M. Knight, Cyclic compression of chondrocytes modulates a purinergic calcium signalling pathway in a strain rate- and frequency-dependent manner, J. Cell. Physiol. 209 (2006) 389–397.
[54] C.T. Hung, F.D. Allen, K.D. Mansfield, I.M. Shapiro, Extracellular ATP modulates $[Ca^{2+}]_i$ in retinoic acid-treated embryonic chondrocytes, Am. J. Physiol. 272 (1997) C1611–C1617.
[55] C.J. O'Conor, H.A. Leddy, H.C. Benefield, W.B. Liedtke, F. Guilak, TRPV4-mediated mechanotransduction regulates the metabolic response of chondrocytes to dynamic loading, Proc. Natl. Acad. Sci. U. S. A 111 (2014) 1316–1321.
[56] W. Lee, H.A. Leddy, Y. Chen, S.H. Lee, N.A. Zelenski, A.L. McNulty, J. Wu, K.N. Beicker, J. Coles, S. Zauscher, J. Grandl, F. Sachs, F. Guilak, Synergy between Piezo1 and Piezo2 channels confers high-strain mechanosensitivity to articular cartilage, Proc. Natl. Acad. Sci. U. S. A. 111 (2014) E5114–E5122.
[57] S.J. Millward-Sadler, M.O. Wright, P.W. Flatman, D.M. Salter, ATP in the mechanotransduction pathway of normal human chondrocytes, Biorheology 41 (2004) 567–575.
[58] M. Lv, Y. Zhou, X. Chen, L. Han, L. Wang, X.L. Lu, Calcium signaling of in situ chondrocytes in articular cartilage under compressive loading: roles of calcium sources and cell membrane ion channels, J. Orthop. Res. 36 (2017) 730–738.
[59] P. Julkunen, W. Wilson, J.S. Jurvelin, R.K. Korhonen, Composition of the pericellular matrix modulates the deformation behaviour of chondrocytes in articular cartilage under static loading, Med. Biol. Eng. Comput 47 (2009) 1281–1290.
[60] P.H. Chao, A.C. West, C.T. Hung, Chondrocyte intracellular calcium, cytoskeletal organization, and gene expression responses to dynamic osmotic loading, Am. J. Physiol. Cell Physiol 291 (2006) C718–C725.
[61] W.A. Hing, A.F. Sherwin, C.A. Poole, The influence of the pericellular microenvironment on the chondrocyte response to osmotic challenge, Osteoarthritis Cartilage 10 (2002) 297–307.
[62] H. Jia, X. Ma, W. Tong, B. Doyran, Z. Sun, L. Wang, X. Zhang, Y. Zhou, F. Badar, A. Chandra, X.L. Lu, Y. Xia, L. Han, M. Enomoto-Iwamoto, L. Qin, EGFR signaling is critical for maintaining the superficial layer of articular cartilage and preventing osteoarthritis initiation, Proc. Natl. Acad. Sci. U. S. A 113 (2016) 14360–14365.
[63] Q. Li, B. Han, C. Wang, W. Tong, W.J. Tseng, L.H. Han, X.S. Liu, M. Enomoto-Iwamoto, R.L. Mauck, L. Qin, R.V. Iozzo, D.E. Birk, L. Han, Mediation of cartilage matrix degeneration and fibrillation by decorin in post-traumatic osteoarthritis, Arthritis Rheumatol (2020) In press, doi:10.1002/art.41254.
[64] M.A. McLeod, R.E. Wilusz, F. Guilak, Depth-dependent anisotropy of the micromechanical properties of the extracellular and pericellular matrices of articular cartilage evaluated via atomic force microscopy, J. Biomech 46 (2013) 586–592.
[65] L. Han, E.H. Frank, J.J. Greene, H.-Y. Lee, H.-H.K. Hung, A.J. Grodzinsky, C. Ortiz, Time-dependent nanomechanics of cartilage, Biophys. J 100 (2011) 1846–1854.
[66] B. Han, H.T. Nia, C. Wang, P. Chandrasekaran, Q. Li, D.R. Chery, H. Li, A.J. Grodzinsky, L. Han, AFM-nanomechanical test: an interdisciplinary tool that links the understanding of cartilage and meniscus biomechanics, osteoarthritis degeneration and tissue engineering, ACS Biomater. Sci. Eng 3 (2017) 2033–2049.